Tuning the Competition between Ferromagnetism and Antiferromagnetism in a Half-Doped Manganite through Magnetoelectric Coupling

Di Yi,[1,*] Jian Liu,[1,2,†] Satoshi Okamoto,[3] Suresha Jagannatha,[4] Yi-Chun Chen,[5] Pu Yu,[6] Ying-Hao Chu,[7] Elke Arenholz,[8] and R. Ramesh[1,‡]

[1]*Department of Materials Science and Engineering and Department of Physics, University of California, Berkeley, California 94720, USA*
[2]*Materials Sciences Division, Lawrence Berkeley National Laboratory, Berkeley, California 94720, USA*
[3]*Materials Science and Technology Division, Oak Ridge National Laboratory, Oak Ridge, Tennessee 37831, USA*
[4]*National Center for Electron Microscopy, Lawrence Berkeley National Laboratory, Berkeley, California 94720, USA*
[5]*Department of Physics, National Cheng Kung University, Tainan 701, Taiwan*
[6]*Department of Physics, State Key Laboratory for Low-Dimensional Quantum Physics, Tsinghua University, Beijing 100084, People's Republic of China*
[7]*Department of Materials Science and Engineering, National Chiao Tung University, Hsinchu 30010, Taiwan*
[8]*Advanced Light Source, Lawrence Berkeley National Laboratory, Berkeley, California 94720, USA*

(Received 27 March 2013; revised manuscript received 22 July 2013; published 18 September 2013)

We investigate the possibility of controlling the magnetic phase transition of the heterointerface between a half-doped manganite $La_{0.5}Ca_{0.5}MnO_3$ and a multiferroic $BiFeO_3$ (BFO) through magnetoelectric coupling. Using macroscopic magnetometry and element-selective x-ray magnetic circular dichroism at the Mn and Fe L edges, we discover that the ferroelectric polarization of BFO controls simultaneously the magnetization of BFO and $La_{0.5}Ca_{0.5}MnO_3$ (LCMO). X-ray absorption spectra at the oxygen K edge and linear dichroism at the Mn L edge suggest that the interfacial coupling is mainly derived from the superexchange between Mn and Fe t_{2g} spins. The combination of x-ray absorption spectroscopy and mean-field theory calculations reveals that the d-electron modulation of Mn cations changes the magnetic coupling in LCMO, which controls the enhanced canted moments of interfacial BFO via the interfacial coupling. Our results demonstrate that the competition between ferromagnetic and antiferromagnetic instability can be modulated by an electric field at the heterointerface, providing another pathway for the electrical field control of magnetism.

DOI: 10.1103/PhysRevLett.111.127601 PACS numbers: 77.55.Nv, 73.20.−r, 75.85.+t, 78.70.Dm

Over the past few years, complex oxide heterointerfaces have been extensively studied due to the novel phenomena that emerge at such interfaces and differ from the individual bulk components of the heterostructure [1–3]. Particularly, there has been a burst of activity to understand the intriguing interfacial magnetoelectric coupling [4–7] in heterostructures consisting of ferroelectric (FE) or multiferroic insulator and ferromagnetic (FM) metal. By controlling the FE polarization and the underlying charge degree of freedom, one can manipulate the spin and orbital degrees of freedom [8–11] and achieve magnetoelectric coupling across the interfaces.

One model heteroepitaxial interface is comprised of the FM $La_{0.7}Sr_{0.3}MnO_3$ (LSMO) juxtaposed with the multiferroic $BiFeO_3$ (BFO). Previous studies on this model heterostructure have reported the emergence of enhanced, interfacial ferromagnetism in BFO and the possibility for interfacial orbital reconstruction in the manganite [12]. Furthermore, it was shown that the FE polarization controls the magnetization and magnetic anisotropy of FM manganite [13]. Within the broader framework of electric field control of magnetism, an interesting question can be put forward: Besides controlling the magnetization direction and magnetic anisotropy of the ferromagnet, can one reversibly switch an antiferromagnet (with no macroscopic magnetic moment) to a ferromagnet (with a macroscopically sensible moment)? This is the central focus of this Letter.

There are some logical criteria that can be used as design rules to accomplish this. First of all, it is desirable in these materials that ferromagnetism strongly competes with antiferromagnetic (AFM) ordering. Moreover, the competition should depend on external fields, such as electric or magnetic field, chemical potential, or strain [14–16]. One ideal candidate is half-doped manganite, exemplified by $La_{0.5}Ca_{0.5}MnO_3$ (LCMO). Bulk LCMO undergoes two successive transitions: a paramagnetic to FM transition followed by a FM to AFM transition [17]. Moreover, the transition is controllable by the magnetic field. These facts clearly characterize the strong competition between FM and AFM order. Recently, Yin *et al.* observed an electrically controllable tunneling resistance by inserting a thin (1–5 uc) LCMO barrier in the junction of LSMO/$BaTiO_3$/LSMO [18]. While it suggests an intriguing possibility to ferroelectrically induce a metal-insulator phase transition in LCMO, direct evidence for a ferroelectrically controllable AFM-FM transition has not been reported.

Here we report ferroelectric control of the AFM-FM transition at the heterointerface between LCMO and BFO. The large FE polarization of BFO provides a possible pathway to reversibly control the magnetic coupling of both the LCMO and BFO [schematic in Fig. 1(a)]. The combination of magnetometry and x-ray magnetic circular dichroism (XMCD) shows that the magnetizations of both LCMO and BFO at the interface are modulated significantly through the reversal of the FE polarization. X-ray absorption spectra (XAS) at the oxygen K edge and linear dichroism (XLD) at the Mn L edge suggest that the main interfacial coupling is derived from the AFM superexchange between Fe and Mn t_{2g} spins. Furthermore, XAS reveals a modulation of the Mn $3d$ electron occupancy due to the charge accumulation. Mean-field theory calculations suggest that the occupancy of Mn e_g electrons controls the magnetic coupling, thus tuning the competition between FM and AFM instability.

LCMO/BFO (5 nm/100 nm) heterostructures [structure $H1$, Fig. 1(a)] were prepared on TiO_2-terminated $SrTiO_3$ (001) substrate by pulsed laser deposition. Reflection high-energy electron diffraction was employed to achieve atomic scale control of the heterointerface. An atomically flat interface was observed by high-resolution scanning transmission electron microscopy (Fig. S1 [19]). The magnetization of the heterostructures was measured by SQUID magnetometry. XAS was acquired by recording the total electron yield (TEY) current as a function of x-ray photon energy at beam line 4.0.2 of the Advanced Light Source at Lawrence Berkeley National Laboratory. Taking into account the surface sensitivity (with a 30° grazing angle) and element selectivity of the TEY mode, XMCD was used to probe the element-resolved magnetic moments in the heterostructure. XLD was measured to study the orbital occupancy.

The FE polarization states of BFO were studied by piezoresponse force microscopy (PFM). A metal-probe setup with a 50 μm tip was used to switch the polarization of the whole sample [Fig. 1(a)]. The dark contrast of the out-of-plane (OOP) image indicates that polarization points away from the interface [$P1$ state, Fig. 1(c)], and the light contrast corresponds to the polarization towards the interface [$P2$ state, Fig. 1(d)]. PFM taken at multiple randomly selected regions confirms a nearly 100% polarization control.

By virtue of the well-controlled FE polarization, we measured the resulting change of the macroscopic magnetization. In Fig. 2, the black (line with solid square), red (line with solid circle), and blue (line with half-filled diamond) curves show the magnetization of the heterostructure [$H1$, Fig. 1(a)] in the as-grown state ($P1$), switched to the opposite state ($P2$) by positive voltage, and switched back to the original state ($P1$) by negative voltage. Reference data from a sample with 100 nm BFO on $SrTiO_3$, which accounts for the diamagnetic signal of the substrate and the small bulk canted moments of BFO [20,21], were subtracted from the raw data (Fig. S3 [19]). The temperature dependence of magnetization in the $P1$ state shows a negligibly small moment. On the other hand, magnetization of the $P2$ state shows a macroscopically sensible moment. The saturationlike behavior between 100 and 200 K suggests FM clusters or canted AFM ordering [22,23]. Furthermore, the data clearly show that the modulation effect is reversible through FE switch. In order to identify the contribution from LCMO and BFO, respectively, we utilized element-specific XAS and XMCD to study the Fe and Mn L edge.

Figures 3(a)–3(d) display the XAS and XMCD at the Mn and Fe L edge at 20 K with an applied field of 0.5 T. Because of the limited probing depth, the heterostructure with a 100 nm BFO top layer ($H1$) is not suitable to study the interface. Therefore, we grew the reversed heterostructure [$H2$, Fig. 1(b)] of the BFO (100 nm, bottom) and LCMO (5 nm/2 nm, top). In the $H2$ structure, the TEY

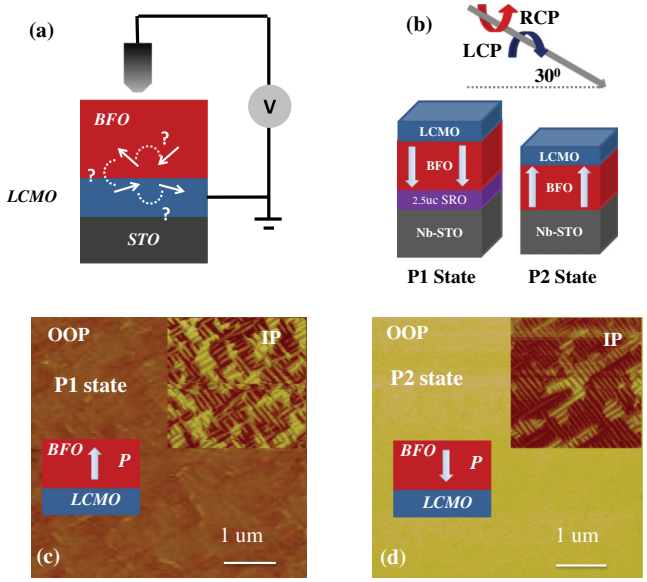

FIG. 1 (color online). Schematic of the heterostructures: (a) structure $H1$ for ferroelectric switch, (b) structure $H2$ for XAS, XMCD, and XLD; (c), (d) PFM of $H1$ structure in $P1$ and $P2$ states.

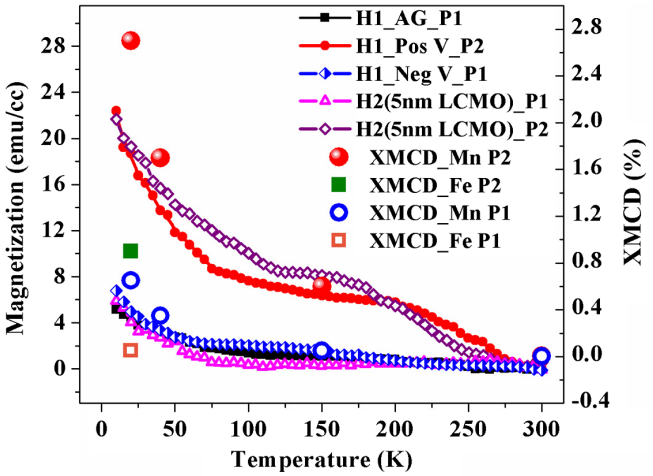

FIG. 2 (color online). Temperature dependence of magnetization of $P1$ and $P2$ states taken with a magnetometer and calculated with the spin sum rule of XMCD.

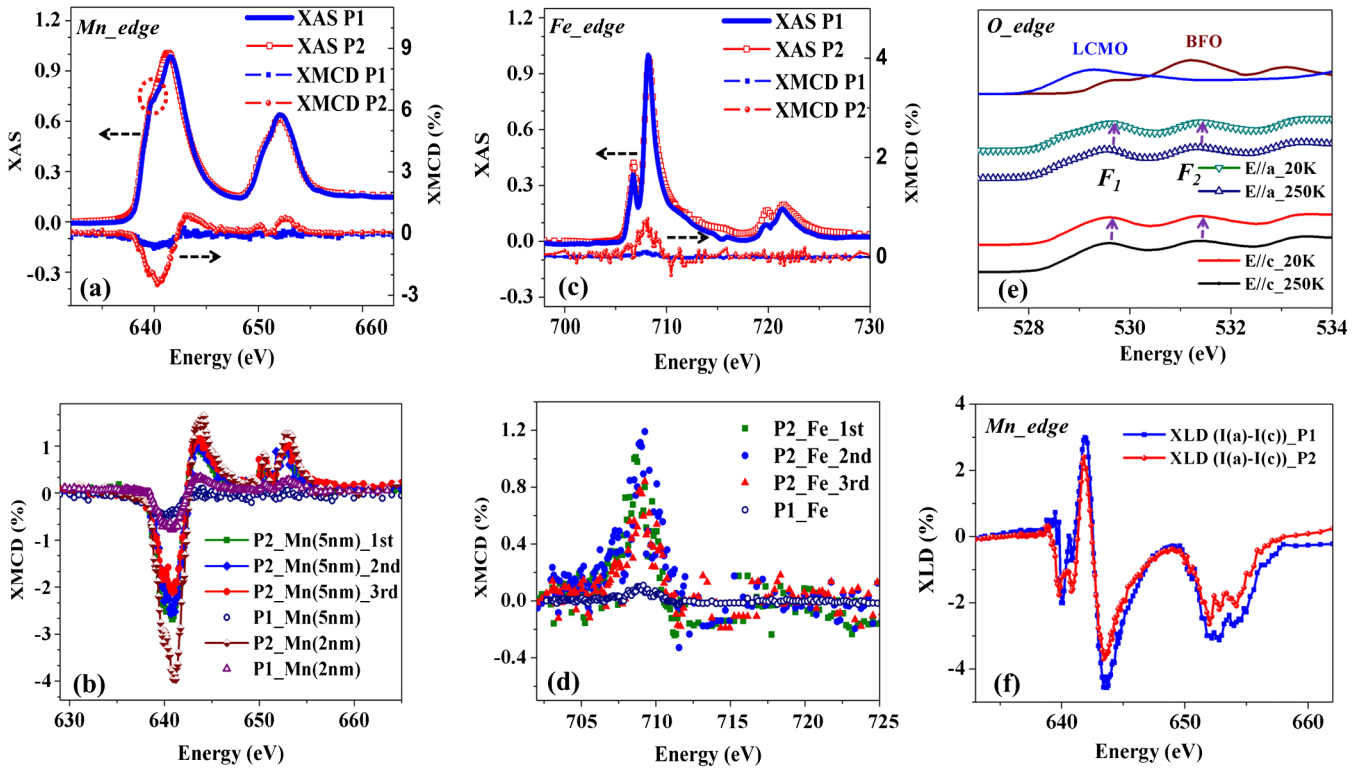

FIG. 3 (color online). (a), (c) The XAS and XMCD spectra of the Mn, Fe $L_{2,3}$ edge in $P1$ and $P2$ states; (b), (d) multiple repeats of XMCD of the Mn, Fe $L_{2,3}$ edge; (e) XAS of the oxygen K edge with linear polarized x ray; (f) XLD spectra of the Mn $L_{2,3}$ edge [I(a) and I(c) correspond to XAS measured with in-plane and out-of-plane polarization, respectively]. XLD is measured at 300 K, where the magnetic dichroic effect is absent. All the data are taken from $H2$ (5 nm LCMO) except (b).

signal comes from the entire LCMO layer and the interfacial BFO. Our previous study demonstrated that the FE polarization can be controlled through the electrostatic boundary condition in the as-grown state [24], which is also confirmed in the $H2$ structures (Fig. S2 [19]). Thus we can study the XAS and XMCD in the two FE states, i.e., $P1$ and $P2$. Magnetization taken with a magnetometer shows the same modulation effects in the $H2$ structure (5 nm LCMO) (Fig. 2). The XMCD of ~2.6% at the Mn L edge is clearly observed in the $P2$ state [Fig. 3(a)], which was confirmed in multiple samples [Fig. 3(b)]. However, no clear XMCD is observed in the $P1$ state. In addition, XMCD of the Fe L edge also reveals a significant change (~1% in the $P2$ state and negligible in the $P1$ state, Figs. 3(c) and 3(d)]. The opposite sign of XMCD signifies an AFM coupling between Fe and Mn across the interface. The temperature dependence of XMCD is summarized in Fig. 2. The magnitude of the magnetization can be quantitatively estimated by the XMCD spin sum rule (Fig. S4 [19]). The obtained value is roughly 0.25 μ_b/Mn for LCMO and 0.1 μ_b/Fe for BFO in the $P2$ state at 20 K. Considering the AFM coupling of Fe and Mn across the interface, the calculated value is in reasonable agreement with the SQUID magnetometry. Furthermore, the XMCD of the $H2$ structure with 2 nm LCMO (~ 4%) is larger than that of the $H2$ structure with 5 nm LCMO [Fig. 3(b)], which suggests that the enhanced moments are mainly from the interface. Interestingly, despite the clear magnetization modulation, the transport property does not display significant variation for the $P1$ and $P2$ states (Fig. S5(d) [19]), unlike that of the tunneling structure studied by Yin *et al.* [18].

Although the enhanced canted moment of BFO has been studied in the LSMO/BFO interface [12], the electrically controllable Fe edge XMCD has not been reported before. In order to gain further insight, we studied the microscopic magnetic coupling across the Fe-O-Mn bond. Figure 3(e) shows the XAS of the oxygen K edge by using linear polarized x ray at different temperatures (similar for $P1$ and $P2$, Fig. S6 [19]). The feature $F1$ corresponds to the mixture of Fe (t_{2g}) and Mn (t_{2g} and e_g) states, and $F2$ is related to only the e_g levels of BFO. A previous study [12] observed that the $F2$ peak shifts to lower energy as the temperature decreases in LSMO/BFO when the x-ray polarization is out of plane, which is explained as the hybridization of the Mn and Fe $3z^2$-r^2 orbital at the interface. However, this shift is absent in Fig. 3(e). In contrast to LSMO, LCMO is under stronger tensile strain from the substrate, resulting in the stabilization of the x^2-y^2 orbital compared with $3z^2$-r^2, which is supported by the negative sign of XLD [I(a)–I(c)] at the Mn L edge [25] [Fig. 3(f)]. Therefore, the orbital reconstruction proposed for the BFO/LSMO interface is not expected here. Instead, we speculate that the main magnetic coupling is derived from the AFM SE between Fe and Mn t_{2g} spins.

Based on the element-specific technique above, we found that the modulation effect is derived from both LCMO and BFO. We speculate that the FE polarization is likely to favor the FM (AFM) coupling in LCMO in the $P2$ ($P1$) state due to the change of d-electron density [8]. The varied magnetic coupling in LCMO then leads to the change of canted moments in the interfacial BFO due to the magnetic coupling. Besides the carrier modulation, the strain effect should also be considered. The strain controlled nonvolatile magnetoelectric coupling requires the change of FE domain and thus the in-plane lattice constant [26]. However, both $P1$ and $P2$ states in this study show similar four-variant domains, which suggests that strain is not likely to be the main reason for the observed nonvolatile magnetization modulation.

To test the electronic origin, we performed a close examination of the XAS spectra of the Mn L edge in the two polarization states [Fig. 3(a)]. Although the XAS of the Mn L edge is similar to a $+3/+4$ mixed valence in both cases, there are a few clear differences between the two states. In particular, the XAS spectrum of the $P1$ state (blue, solid line) shows an enhanced shoulderlike feature on the low-energy side of the main peak of the L_3 edge, which is highly suppressed in the spectrum of the $P2$ state (red, solid line with open square symbol). Besides, the main absorption peak shifts to the higher energy level in the $P1$ state comparing with the $P2$ state by roughly 0.2 eV. Previous studies on manganite revealed that both the peak position and the line shape of the Mn L edge XAS are highly sensitive to the Mn valence state [27,28]. It has been demonstrated that the peak energy increases for a higher oxidation state of Mn, and the enhanced shoulderlike multiplet structure of the L_3 edge is the fingerprint of the Mn^{4+} state. Moreover, the change of the L_3/L_2 ratio follows the trend demonstrated in previous studies [29], which suggests higher oxidation state in the $P1$ state. Therefore, by taking all these observations into account, we can reach a conclusion that the valence state of Mn changes due to the carrier modulation by the FE polarization. The valence state of $P1$ is closer to Mn^{4+}, while the valence state of $P2$ is driven toward Mn^{3+}. Based on the energy shift [30], we estimate an average change of the Mn valence to be $\sim 0.1/\mathrm{Mn}$, consistent with the calculated average change of charge of $0.11e/\mathrm{Mn}$, assuming $2P_s = 130\ \mu\mathrm{C/cm^2}$ [31]. Since the modulated charge density is expected to decay away from the interface, the interface region may have a carrier density higher than the average, which could result in the relatively high onset temperature of the magnetic moments in the $P2$ state similar to that of $La_{0.7}Ca_{0.3}MnO_3$. Quantifying the exact depth profile of charge and magnetic moment of this kind of heterostructure is an interesting subject for further study.

To quantify the relationship between the densities of e_g electrons and the magnetic interactions in LCMO, we then performed mean-field theory calculations. Here we consider a two-dimensional double-exchange (DE) model with e_g orbitals and superexchange (SE) between neighboring t_{2g} spins. The details of the model are described in the Supplemental Material [Fig. S7(a) [19]]. The competition between SE coupling (JS^2) and DE (t) is represented by their ratio JS^2/t. For each value of JS^2/t, the relative angle θ_2 between neighboring spins across the zigzag chain was obtained by solving for the minimum of free energy. ($\theta_2 = 0/\pi$ corresponds to the FM/CE-type AFM spin arrangement.) We estimate the critical value of JS^2/t to be slightly larger than 0.112, which reproduces the CE-AFM ground state with orbital ordering for $N = 0.5$ [Fig. S7(b) [19]], consistent with previous studies [32–34]. Figures 4(a) and 4(b) present the results for hole doping ($N = 0.45$) and electron doping ($N = 0.55$), respectively. The results show that canting of antiferromagnetically coupled neighboring moments is possible for both electron and hole doping. However, the canting is stronger in the electron-doping than the hole-doping side. The results suggest that the FM ordering is energetically more favorable at the critical value of JS^2/t when electrons are accumulated in LCMO, which is in accordance with the macroscopic moments observed by both the magnetometry and XMCD in the $P2$ state. On the other hand, the AFM coupling is energetically more favorable in the hole-doping side. Based on these considerations, we propose a mechanism for the electrical control of magnetic coupling at the BFO/LCMO heterointerface as shown schematically in Fig. 4(c). The FM

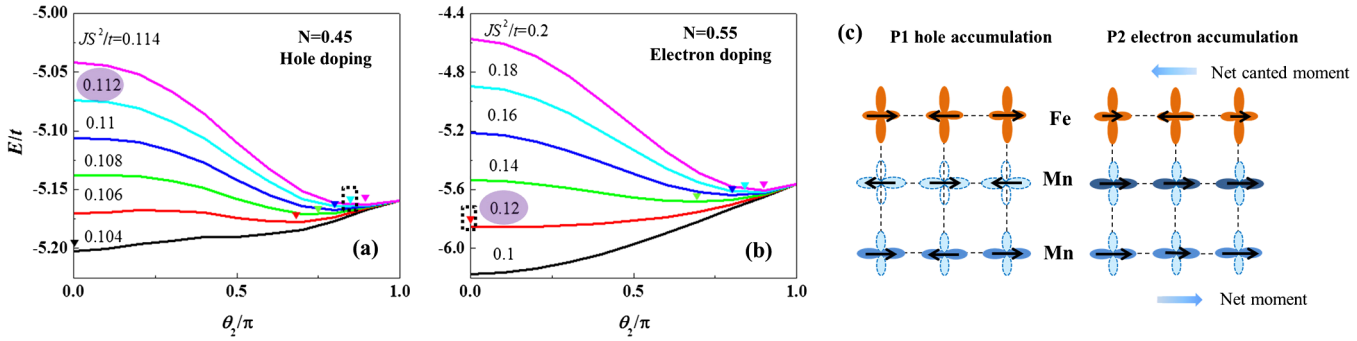

FIG. 4 (color online). Mean-field theory calculations on the relationship between e_g electron density (N) and spin structure for hole (a) and electron (b) doping of LCMO (θ_2 is the relative angle between neighboring spins across the zigzag chain); (c) schematic of the electron density and spin structure at the heterointerfaces (the dark-light contrast suggests the electron accumulation or depletion).

interaction in LCMO is enhanced by electron doping. The magnetic coupling across the heterointerface then leads to the larger canted moments in BFO. Oppositely, both LCMO and BFO remain AFM in the hole-doping side. Our microscopic mechanism consistently explains the modulated competition between FM and AFM instability by switching FE polarization.

In summary, we have demonstrated the ability to modulate the competition between FM and AFM instability through magnetoelectric coupling at the BFO/LCMO heterointerface. The magnitude of magnetization in both the interfacial BFO and LCMO changes dramatically in response to the FE polarization switch. The magnetoelectric coupling is derived from the charge modulation and the interplay between charge and spin degree of freedom both in the layer and across the interface. Our results suggest a possible route to explore the reversible electrical switch between an antiferromagnet and a ferromagnet. Indeed, we believe that there may be other similar pathways by which an AFM state can be reversibly switched into a FM state, through local electronic structure modulations.

The authors acknowledge fruitful discussions with G. Bhalla, J. H. Chu, and G. Palsson. Research at Berkeley was sponsored by the National Science Foundation through the Penn State MRSEC. J. L. thanks the support from the Quantum Material program in the Materials Sciences Division in Lawrence Berkeley National Laboratory. The work at ORNL was supported by the U.S. Department of Energy, Basic Energy Sciences, Materials Sciences and Engineering Division. The work at National Chiao Tung University was supported by the National Science Council, R. O. C. (NSC-1012119-M-009003-MY2), Ministry of Education, R. O. C. (MOE-ATU 101W961), and Center for interdisciplinary science of National Chiao Tung University.

*yid@berkeley.edu
†jian.liu@berkeley.edu
‡Present address: Oak Ridge National Laboratory, Oak Ridge, TN 37831, USA.

[1] H. Y. Hwang, Y. Iwasa, M. Kawasaki, B. Keimer, N. Nagaosa, and Y. Tokura, Nat. Mater. **11**, 103 (2012).
[2] P. Zubko, S. Gariglio, M. Gabay, P. Ghosez, and J.-M. Triscone, Annu. Rev. Condens. Matter Phys. **2**, 141 (2011).
[3] J. Chakhalian, A. J. Millis, and J. Rondinelli, Nat. Mater. **11**, 92 (2012).
[4] W. Eerenstein, N. D. Mathur, and J. F. Scott, Nature (London) **442**, 759 (2006).
[5] S. W. Cheong and M. Mostovoy, Nat. Mater. **6**, 13 (2007).
[6] R. Ramesh and N. A. Spaldin, Nat. Mater. **6**, 21 (2007).
[7] M. Fiebig, J. Phys. D **38**, R123 (2005).
[8] C. A. F. Vaz, J. Hoffman, Y. Segal, J. W. Reiner, R. D. Grober, Z. Zhang, C. H. Ahn, and F. J. Walker, Phys. Rev. Lett. **104**, 127202 (2010).
[9] J. Burton and E. Tsymbal, Phys. Rev. B **80**, 174406 (2009).
[10] S. M. Wu, S. A. Cybart, P. Yu, M. D. Rossell, J. X. Zhang, R. Ramesh, and R. C. Dynes, Nat. Mater. **9**, 756 (2010).
[11] S. M. Wu, S. A. Cybart, D. Yi, J. M. Parker, R. Ramesh, and R. C. Dynes, Phys. Rev. Lett. **110**, 067202 (2013).
[12] P. Yu *et al.*, Phys. Rev. Lett. **105**, 027201 (2010).
[13] P. Yu *et al.* (unpublished).
[14] Y. Tokura, Rep. Prog. Phys. **69**, 797 (2006).
[15] C. Cui, T. A. Tyson, Z. Chen, and Z. Zhong, Phys. Rev. B **68**, 214417 (2003).
[16] P. Ryan *et al.*, Nat. Commun. **4**, 1334 (2013).
[17] P. Radaelli, D. E. Cox, M. Marezio, and S. W. Cheong, Phys. Rev. B **55**, 3015 (1997).
[18] Y. W. Yin *et al.*, Nat. Mater. **12**, 397 (2013).
[19] See Supplemental Material at http://link.aps.org/supplemental/10.1103/PhysRevLett.111.127601 for details of sample preparation, structural characterization, magnetic and electronic measurements, and the model of the mean-field theory calculations.
[20] C. Ederer and N. Spaldin, Phys. Rev. B **71**, 060401(R) (2005).
[21] H. Ba *et al.*, Appl. Phys. Lett. **87**, 072508 (2005).
[22] I. Solovyev and K. Terakura, Phys. Rev. B **63**, 174425 (2001).
[23] H. Kawano, R. Kajimoto, M. Kubota, and H. Yoshizawa, Phys. Rev. B **53**, 2202 (1996).
[24] P. Yu *et al.*, Proc. Natl. Acad. Sci. U.S.A. **109**, 9710 (2012).
[25] D. Pesquera, G. Herranz, A. Barla, E. Pellegrin, F. Bondino, E. Magnano, F. Sánchez, and J. Fontcuberta, Nat. Commun. **3**, 1189 (2012).
[26] S. Zhang *et al.*, Phys. Rev. Lett. **108**, 137203 (2012).
[27] J. Lee *et al.*, Phys. Rev. B **80**, 205112 (2009).
[28] Y. Takamura, F. Yang, N. Kemik, E. Arenholz, M. D. Biegalski, and H. M. Christen, Phys. Rev. B **80**, 180417 (R) (2009).
[29] M. Varela, M. Oxley, W. Luo, J. Tao, M. Watanabe, A. Lupini, S. Pantelides, and S. Pennycook, Phys. Rev. B **79**, 085117 (2009).
[30] S. P. Cramer, F. M. F. DeGroot, Y. Ma, C. T. Chen, F. Sette, C. A. Kipke, D. M. Eichhorn, M. K. Chan, and W. H. Armstrong, J. Am. Chem. Soc. **113**, 7937 (1991).
[31] J. Li, J. Wang, M. Wuttig, R. Ramesh, N. Wang, B. Ruette, A. P. Pyatakov, A. K. Zvezdin, and D. Viehland, Appl. Phys. Lett. **84**, 5261 (2004).
[32] I. Solovyev and K. Terakura, Phys. Rev. Lett. **83**, 2825 (1999).
[33] J. van den Brink, G. Khaliullin, and D. Khomskii, Phys. Rev. Lett. **83**, 5118 (1999).
[34] S. Okamoto, Phys. Rev. B **82**, 024427 (2010).